

Article

Experimental Investigation of Horizontal Wave Pressure on the Caisson Protected by Armor Blocks on the Rubble-Mounted Core

Sang-Ho Oh *  and Jae-Sung Lee 

Coastal Development and Ocean Energy Research Center, Korea Institute of Ocean Science and Technology, 385 Haeyang-ro, Yeongdo-gu, Busan 49111, Korea; wofmtjd@kiost.ac.kr

* Correspondence: coast.oh@gmail.com; Tel.: +82-51-664-3523

Received: 12 August 2020; Accepted: 3 September 2020; Published: 7 September 2020



Abstract: The horizontal wave pressure on the front wall of the caisson protected by armor blocks on the rubble-mounted core is investigated by carrying out physical experiments. There have been few previous studies regarding this type of structure, and the characteristics of horizontal wave pressure on the structure are still unclear. Considering this, a series of experiments were performed by changing the configuration of the coverage rate in front of the caisson and the shoulder width of the armor blocks. For each of the different configurations of the model setup, wave pressure on the caisson was measured under 20 regular waves of different wave periods and heights. By analyzing the obtained experimental data, it was possible to quantify the effects of the coverage rate and the shoulder width on the wave pressure. The wave pressure tended to increase up to maximally 1.5 to 2 times at the exposed part of the caisson if it was incompletely protected. In addition, the wave pressure at the top part of the caisson was substantially reduced with the increase of the shoulder width of the armor layer. Based on these results, adjustment factors for evaluating such effects have been suggested, which can be applicable for the practical design of the caisson covered with armor blocks on the rubble-mounted core.

Keywords: wave pressure; caisson; horizontally composite breakwater; rubble-mounted core; physical experiment

1. Introduction

Caisson breakwaters are likely to receive impulsive wave loading on their front faces. Hence, estimation of the horizontal wave pressures on the caisson is the most fundamental and important factor for the safe design of the structure. Goda's formula [1,2] is one of the most commonly accepted methods for estimating wave forces on caissons. The formula predicts a maximum pressure at the still water level, p_1 , which is given as follows.

$$p_1 = 0.5(1 + \cos \theta)(\lambda_1 \alpha_1 + \lambda_2 \alpha^* \cos^2 \theta) \rho g H \quad (1)$$

where θ is the wave incidence angle, ρ is the density of the water, g is the gravitational acceleration, λ_1 and λ_2 are modification factors depending on the geometry of a structure, and α_1 and α^* represent the coefficients of the pulsating and impulsive wave pressure, respectively.

In some cases, a number of concrete armor blocks are piled up in front of the caisson to reduce the impulsive wave loading on a caisson, as illustrated in Figure 1, which is referred to as a horizontally

composite breakwater [3]. The horizontal wave pressure on such a caisson can be estimated by adjusting the modification factor λ_1 of Goda's formula [4].

$$\lambda_1 = \begin{cases} 1.0 & (H/h \leq 0.3) \\ 1.2 - 2(H/h)/3 & (0.3 < H/h \leq 0.3) \\ 0.8 & (H/h > 0.3) \end{cases} \quad (2)$$

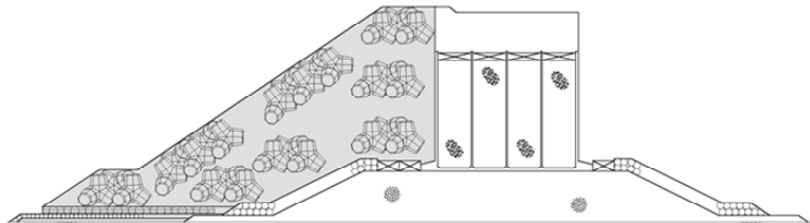


Figure 1. A conceptual diagram of a caisson whose front face is covered with armor blocks on the rubble mound foundation.

The value of λ_1 depends on the ratio of the wave height (H) to the water depth (h), varying from 0.8 to 1.0. It is noteworthy that Equation (2) is exclusively applicable when the upright section of a caisson is fully covered with armor blocks.

In most cases, the crest level of the armor blocks is equal to or slightly higher than the crown of the caisson as in Figure 1. However, occasionally, the upright section of the caisson is not fully covered up to the crown level, for example while construction is in progress or when the armor blocks are settled down or displaced after experiencing repeated wave action [5,6]. In such a case, the horizontal wave force on the structure can be larger than that on the solid caisson without any protection [2]. In addition, impulsive wave loading may act on the top exposed section of the caisson, which leads to possible failure of the structure. Indeed, for instance, the caisson breakwater installed at Mutsu-Ogawara port in Japan was severely damaged in 1991 because the armor blocks in front of the caisson had been scattered by storms, which allowed impulsive wave loading on the disclosed section of the caisson [7,8]. In a laboratory experiment, Takayama et al. [9] reported that settlement of the armor blocks caused an increase of wave force on the caisson. In addition, Mase et al. [10] analyzed the stability of composite breakwater assuming the settlement of armor blocks in front of the breakwater, and they demonstrated that the sliding distance of a caisson was reduced when the settled blocks were repaired. More recently, Oh et al. [6] carried out experiments of measuring wave pressures on a caisson with different coverage rates of tetrapods, showing that the wave force on the caisson significantly increased as the coverage rate decreased.

Based on a reproduction experiment for damaged seawalls due to a typhoon, Takahashi et al. [11] proposed an empirical formula that can be applied for estimating wave pressure on a seawall whose top section is not fully covered with armor blocks. The formula suggests that the pressure distribution along the vertical wall is different depending on the three regions as depicted in Figure 2. In the figure, d_p is the height of Region 2 and defined by Equation (3).

$$d_p = \min\{H_s/3, (R_c - A_c)\} \quad (3)$$

where H_s is the significant wave height measured at the toe of the structure, R_c is the crest freeboard of the caisson, and A_c is the crest level of the armor layer from the still water level.

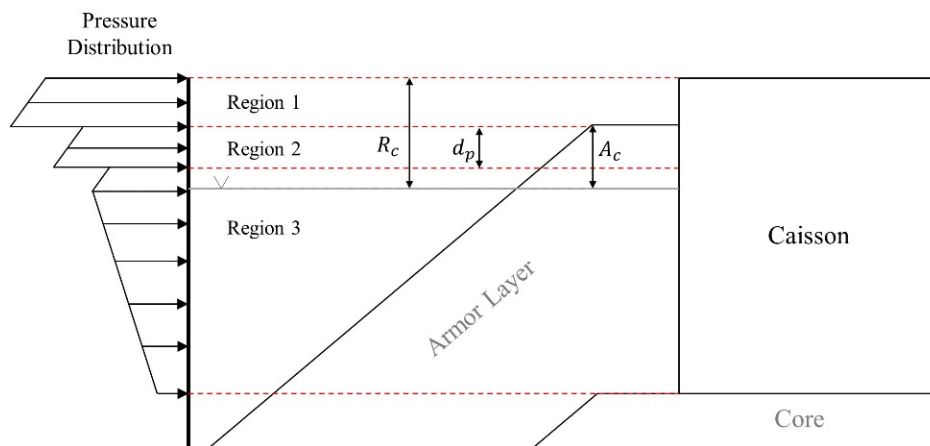


Figure 2. Distribution of wave pressures for each region due to subsidence of blocks.

For each of the three regions, the coefficients of λ_1 or λ_2 of Equation (1) are differently applied. In case of Region 1, $\lambda_1 = 1.0$ and λ_2 is given as follows

$$\lambda_2 = \begin{cases} 1.0 & (A_c/H < 0) \\ 1.0 - 10(A_c/H)/7 & (0 \leq A_c/H \leq 0.7) \\ 0 & (0.7 < A_c/H) \end{cases} \quad (4)$$

For Region 2, λ_1 is given as follows, where λ_{10} is calculated by Equation (2). Meanwhile, λ_2 is obtained the same as Region 1 using Equation (3).

$$\lambda_1 = \lambda_{10}\lambda_{11} \quad (5)$$

$$\lambda_{11} = \begin{cases} 1.0/\lambda_{10} & (A_c/H < 0) \\ \left\{ 1.0 - \frac{1.0-\lambda_{10}}{0.35} \left(\frac{A_c}{H} \right) \right\} / \lambda_{10} & (0 \leq A_c/H \leq 0.35) \\ 1.0 & (0.35 < A_c/H) \end{cases} \quad (6)$$

For Region 3, λ_1 is obtained the same as Region 2, where as $\lambda_2 = 0$.

Meanwhile, another method of reducing wave loading on a caisson is to place the rubble stones in front of the caisson and cover them with armor blocks, as depicted in Figure 3. Regarding this type of horizontally composite breakwater, there exists few previous studies of estimating the wave pressure acting on the structure. In this respect, the present study conducted a series of experiments by changing the configurations of the protection in front of the caisson, and it proposed a method for estimating horizontal wave pressure on the caisson.

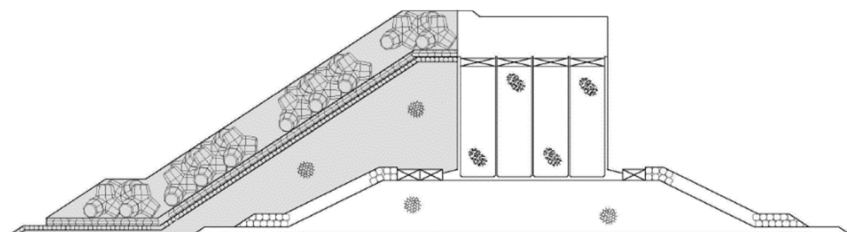


Figure 3. A conceptual diagram of a caisson covered with armor blocks on the rubble-mounted core.

The structure of the paper is as follows. First, details of the experimental setup are described in Section 2. In Section 3, the results of comparison of horizontal wave pressure depending on different coverage rates are presented with a newly suggested formula. In Section 4, the influence of shoulder width of the armor layer is discussed. Finally, conclusions are provided in Section 5.

2. Experimental Setup

The experiments were carried out in a wave flume 50 m long, 1.2 m wide, and 1.6 m deep [12,13]. The wave flume is equipped with a piston-type wave maker, which incorporates a function that actively absorbs the reflected waves. As shown in Figure 4, there is a 1:0.035 slope on the bottom of the flume in the range of 10 to 20 m from one end of the flume. Caisson models made of acrylic plates were placed on the 10 cm high rubble mound that was located at a distance of 28 m from the wave paddle. Figure 5 shows the overall geometry of the model and the definitions of the physical parameters used in this study. The dimensions of the caisson model are 0.45 m long, 0.4 m wide, and either 0.5 or 0.6 m high.

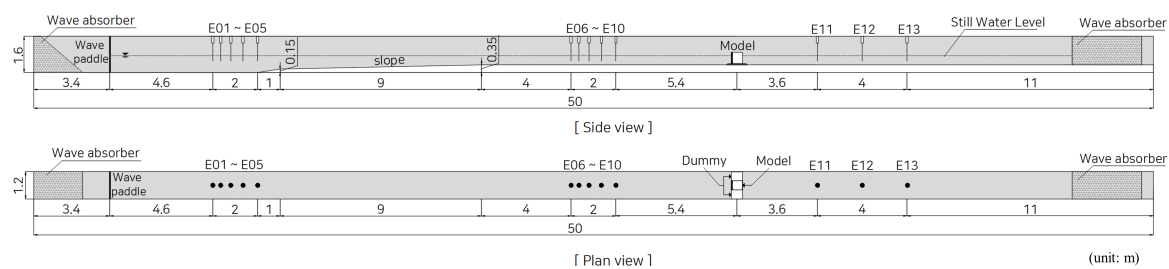


Figure 4. Side and plan views of the wave flume showing the experimental setup. The locations of the caisson model and 13 wave gauges are illustrated in the figure.

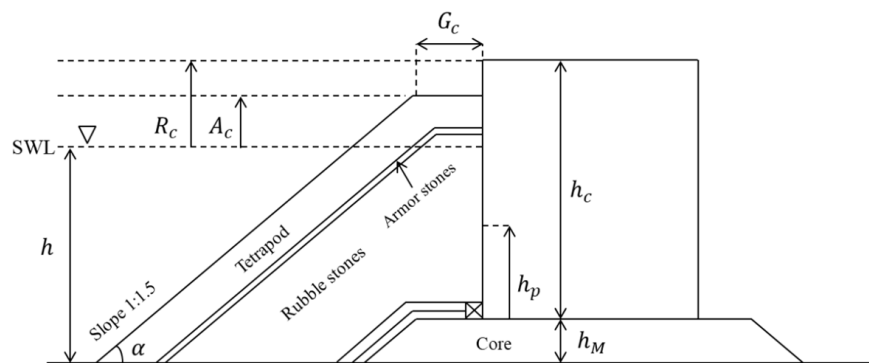


Figure 5. Illustration of the experimental parameters used in the experiment.

Following the measurement techniques used in the previous studies [6,14], horizontal wave loading was measured by using miniscule disk-type pressure transducers. As shown in Figure 6, the pressure transducers were embedded into the center of each plate to measure the horizontal wave pressure. Further details of the technical specification and characteristics of the pressure transducers are described in Oh et al. [6]. As shown in the plan view of Figure 4, two additional dummy caisson models of the same width (0.4 m) were placed on both sides of the caisson model, for which no measurement was made. Meanwhile, water surface displacements were measured by using capacitance wave gauges at 13 locations (E01–E13), as shown in Figure 4.

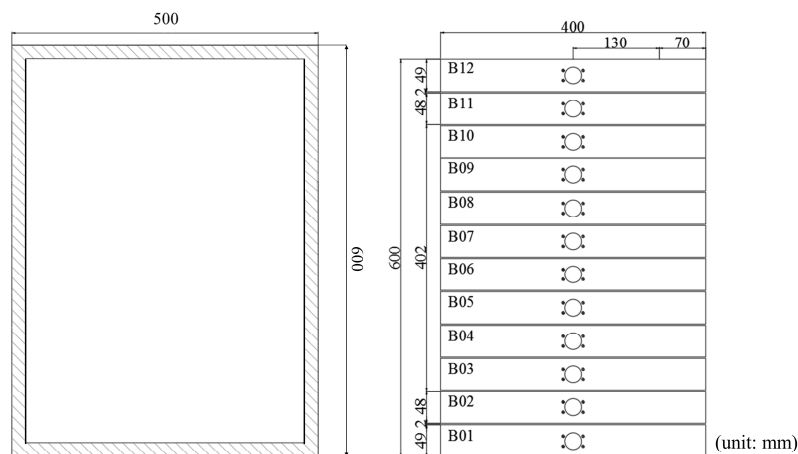


Figure 6. Side view (left) and front view (right) of the caisson model (when $h_c = 0.6$ m).

3. Horizontal Wave Pressure Depending on Different Coverage Rates

3.1. Experimental Conditions with Different Configurations of the Protection in Front of the Caisson

The experiments were conducted with three different caisson models as listed in Table 1. For the three caisson models, horizontal wave pressure on the caisson was measured with four different configurations of the armor blocks on the rubble-mounted core. As illustrated in Figure 7, the case without any protection in front of the caisson is termed as T01. Meanwhile, the case of full coverage of tetrapods on the rubble-mounted core up to the crest level is termed as T11, corresponding to 100% coverage rate ($C_R = 1.0$), which is defined as the rate of the vertical distance protected by tetrapods and rubble stones to the entire caisson height. The cases corresponding to a lack of protection over the top 15% or 30% of the caisson are termed as T12 or T13, whose coverage rate is namely 85% ($C_R=0.85$) or 70% ($C_R=0.7$), respectively. Figure 8 shows two snapshots of the caisson models with the coverage rate of 100% and 70% respectively, which were taken under still water-level conditions right after the preparation of each model.

Table 1. Values of the geometrical parameters of the three test models.

Model ID	h (m)	h_M (m)	h_c (m)	G_c (m)	R_c (m)
C12	0.4	0.10	0.5	0.15	0.20
C13	0.5	0.15	0.5	0.15	0.15
C14	0.5	0.10	0.6	0.15	0.20

In summary, a total of 12 different test cases were considered in the experimental campaign, in terms of the three sets of geometrical parameters shown in Table 1 and the four configurations of the protection in front of the caisson. For instance, the case identification label of C13T12 corresponds to the 0.5 m high caisson model that is placed on the 0.15 m high mound (C13), whose front wall coverage rate is 85% (T12).

Tetrapods made of concrete with a nominal diameter $D_n = 7.5$ cm were regularly placed in two layers, and the fore slope of the armor layers was constant ($\cot \alpha = 1.5$) for all the models. The main interest of this study was to evaluate the effects of coverage rate and the shoulder width on the horizontal wave pressure. Hence, parameters such as D_n and $\cot \alpha$ were not changed for the entire experiment. During the measurement, tetrapods scarcely moved because they were stable even for the maximum wave height. However, if the tetrapods move, they can cause great damage to the pressure transducers, particularly when the top part of the caisson is not protected. For this reason, the armor layers were covered with a thin net that is fixed to the ground and the structure to restrict any possible movement of tetrapods. Meanwhile, rubble stones of $D_{n50} = 8.5$ mm were used to form the core in

front of the caisson model. In addition, rubble stones of $D_{n50} = 18$ mm were used as a middle layer between the core and tetrapods.

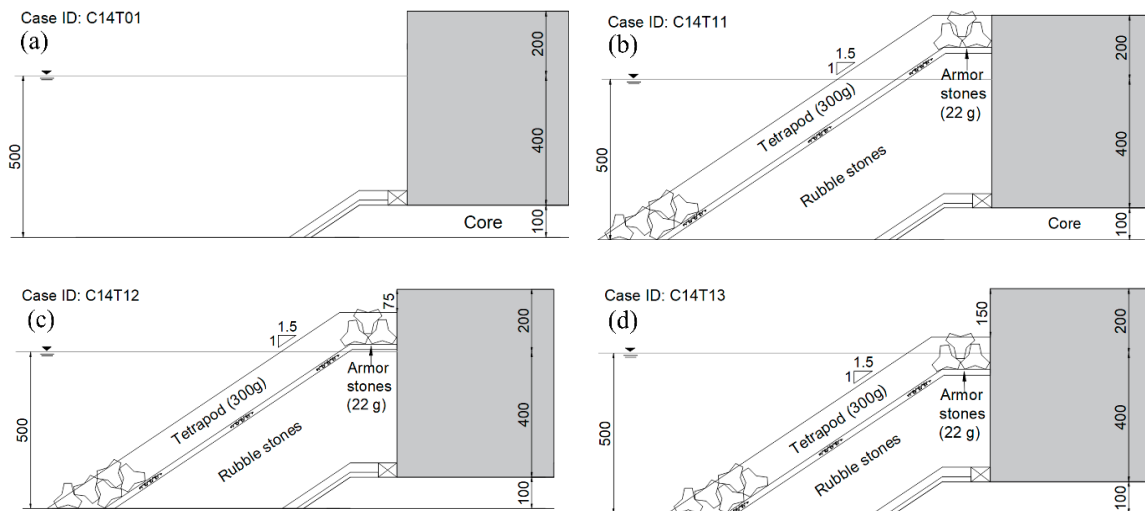


Figure 7. Four different configurations in terms of protection in front of the caisson model of C14. (a) C14T01 (coverage rate: 0%), (b) C14T11 (coverage rate: 100%), (c) C14T12 (coverage rate: 85%), (d) C14T13 (coverage rate: 70%).

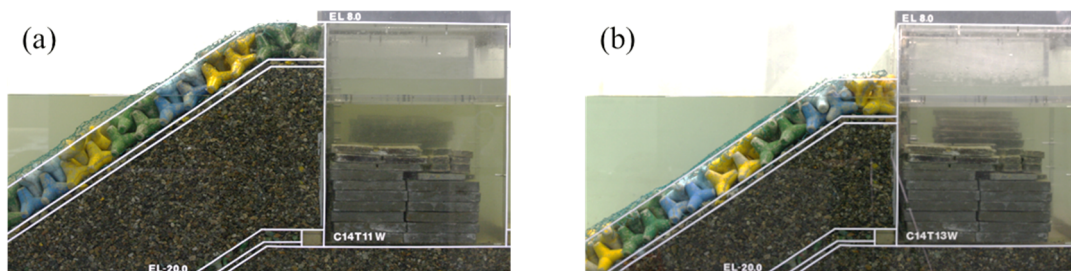


Figure 8. Snapshots of (a) C14T11 and (b) C14T13 models taken before receiving wave action.

For each of the 12 test cases, 20 different regular waves were generated for the measurement. The wave period ranged from 1.5 to 2.5 s at an interval of 0.25 s, while four different wave heights in the range shown in Table 2 were generated for each wave period. Table 2 illustrates the test wave conditions including the wave steepness (s) and the surf similarity parameter (ξ), which is defined as $\xi = \tan \alpha / \sqrt{H/L}$ where α is the angle of the fore slope of the structure. The wave generation time was 60 s for all the cases, during which the data from all the sensors were recorded at a sampling rate of 600 Hz.

Table 2. Summary of the test wave conditions.

h (m)	T (s)	H (m)	s	ξ
0.4	1.5~2.5	0.10~0.25	0.02~0.09	2.13~4.25
0.5	1.5~2.5	0.16~0.33	0.03~0.10	2.07~3.61

3.2. Horizontal Pressure Distributions Depending on the Coverage Rate

Figure 9 shows an example distribution of the measured wave pressure along the caisson according to the four different coverage rates. It is clear that the wave pressure significantly reduced over the entire caisson when it was fully covered with tetrapods and rubble stones. However, when the caisson was partially covered, huge wave pressure acted on the exposed portion of the caisson. More specifically,

the peak pressure appeared at just above the crest level of the armored section. For the C14T12 case, the highest pressure was observed at the top pressure transducer. Meanwhile, the magnitude of measured pressure reached a maximum at the pressure transducer right above the still water level.

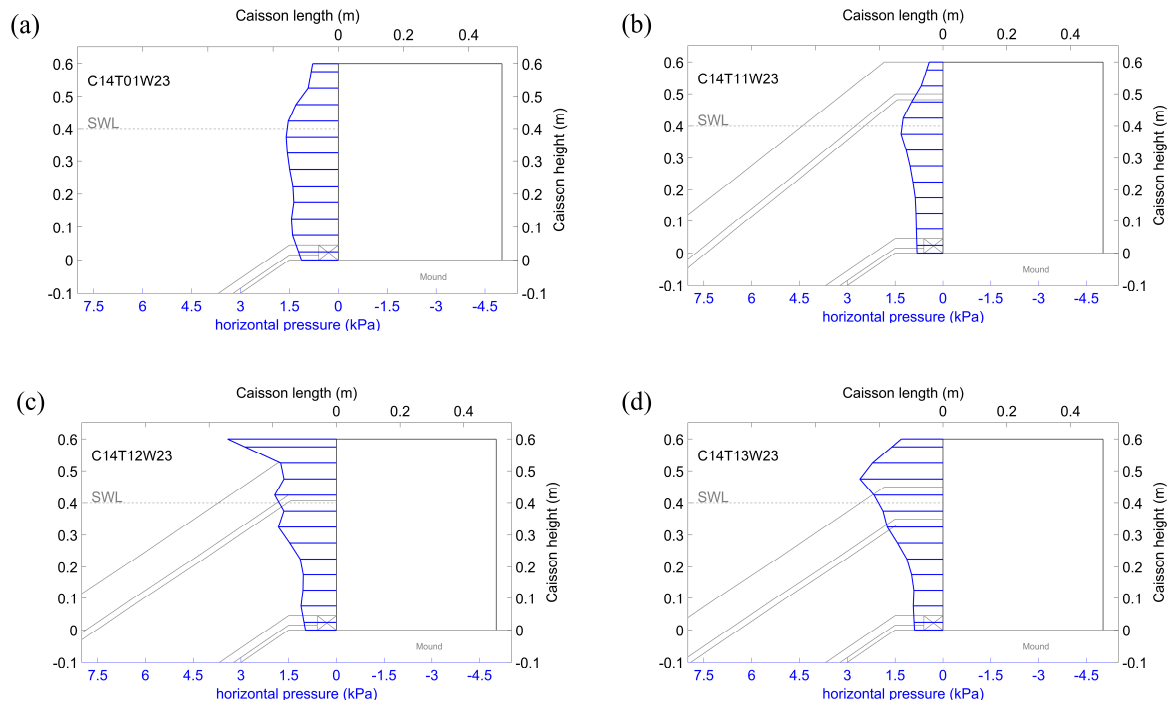


Figure 9. Horizontal wave pressures on the caisson model of C14 for the different coverage rates when $T = 1.5$ s and $H = 0.26$ m. (a) T01, (b) T11, (c) T12, and (d) T13.

Figure 10a shows a comparison of the four pressure distributions illustrated in Figure 9. It is very clear that pressure distribution along the caisson model varied due to the change of the coverage rate. In particular, the horizontal pressures over the upper portion of the caisson showed greater variation depending on the different coverage rates than the lower portion of the caisson. It is noteworthy that the overall magnitude of the wave pressures becomes even larger when the caisson was partially covered (T12 and T13) than when the caisson was uncovered (T01). Such a phenomenon was commonly observed for the rest of test cases, as shown in another example of Figure 10b, where the result for a different wave condition is displayed. The reason for this is due to occurrence of impulsive wave loading on the structure incurred by wave breaking over the fore slope of the caisson when the caisson was partially covered by rubble stones and tetrapods.

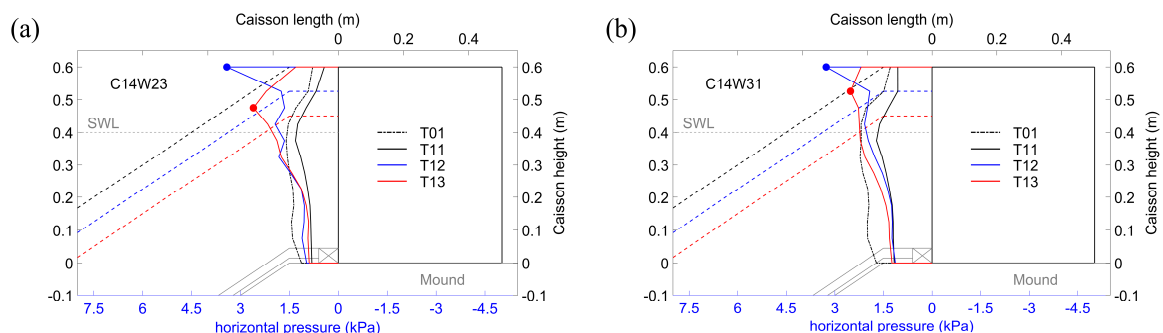


Figure 10. Comparison of the horizontal pressure distributions along the caisson model of C14 according to different coverage rates. (a) $T = 1.5$ s and $H = 0.26$ m, (b) $T = 2.0$ s and $H = 0.26$ m.

3.3. Comparison of Measured Pressures with Takahashi's Formula

As described in the above, Takahashi et al. [11] proposed an empirical formula for calculating the wave pressure on the caisson whose front wall is not fully covered with armor blocks. Although the experimental model in this study, which is compositely covered with armor blocks and rubble stones as well, is different from the structure studied in Takahashi et al. [11], it may be possible to apply this formula because it is the only formula available to estimate the wave pressure on a partially protected caisson. Figure 11 shows two example results of comparing the pressure distribution calculated by the formula with profiles of the measured pressure for the case of C14T12. Takahashi's formula tends to overestimate the measured pressure in Regions 2 and 3, whereas it underestimates the impulsively-acting wave pressure in Region 1. Meanwhile, Figure 12 shows another comparison between the formula and measurement for the case of C14T13. In this case, Takahashi's formula overestimates the wave pressure for entire regions. In particular, the discrepancy between the estimation and measurement is the largest in Region 2.

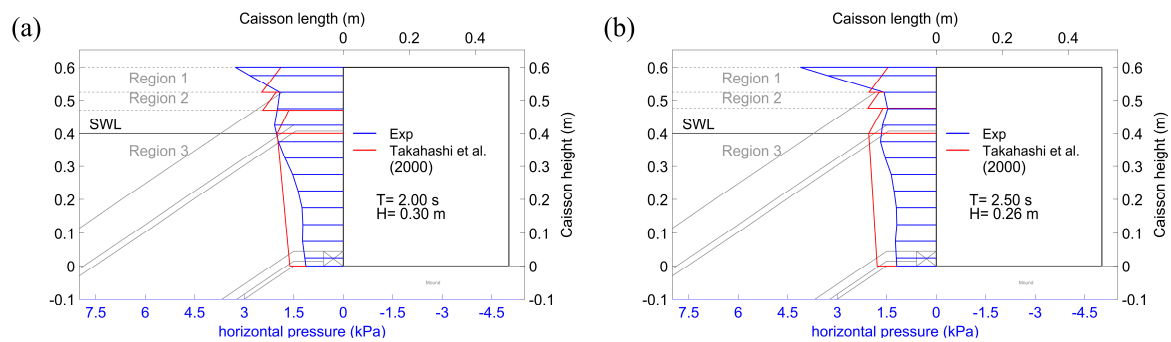


Figure 11. Comparison of the measured horizontal pressure with Takahashi's formula when the coverage rate was 85%. (a) $T = 2.0$ s, $H = 0.30$ m, (b) $T = 2.5$ s, $H = 0.26$ m.

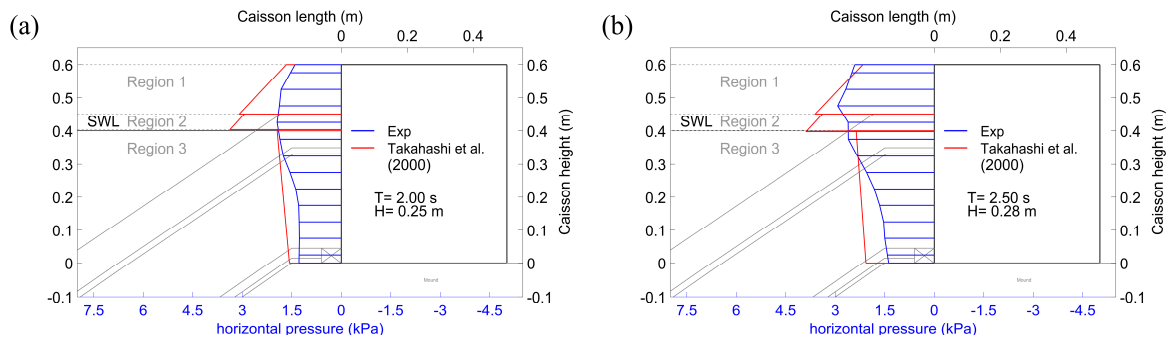


Figure 12. Comparison of the measured horizontal pressure with Takahashi's formula when the coverage rate was 70%. (a) $T = 2.0$ s, $H = 0.29$ m, (b) $T = 2.5$ s, $H = 0.28$ m.

By integrating the pressures over the entire height of the caisson, it was possible to obtain the total horizontal force on the caisson. Then, it is possible to compare the measured force and the calculated force based on Takahashi's formula. Figure 13 shows such a result, where the measured horizontal forces ($F_{H,Measured}$) are compared with the calculated horizontal forces by Takahashi's formula ($F_{H,Takahashi}$) by using all the data from C14 model. It is clear that Takahashi's formula tends to overestimate the measured force regardless of the coverage rate. For the four models shown in Table 1, similar results were obtained that indicate overestimation of the formula to the measured forces.

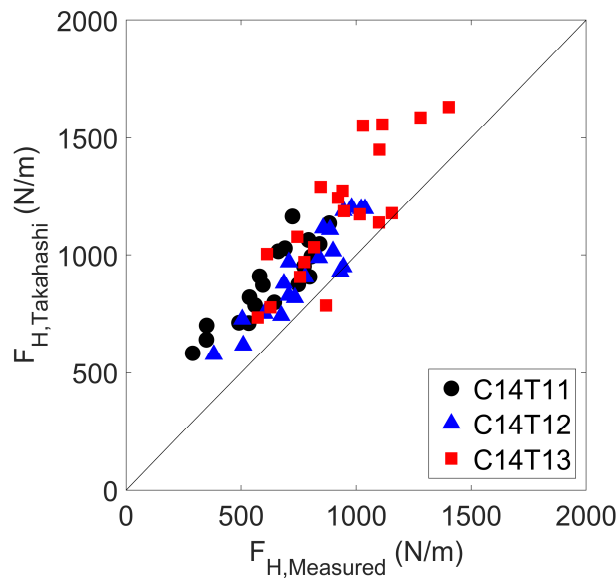


Figure 13. Comparison of horizontal wave forces from the experiments with Takahashi’s formula [11].

3.4. Parameterization of Vertical Profiles of the Horizontal Pressure

Vertical profiles of the horizontal wave pressure on the caisson significantly changed according to the coverage rate, but there exists no adequate formula to estimate such variations of the vertical profiles depending on different coverage rates. Considering this, efforts were made to represent the measured pressure as a function of the relative vertical position along the front wall of the caisson, h_p/h_c , where h_p refers to the vertical distance from the caisson bottom, and h_c refers to the caisson height. Hence, the value of h_p/h_c ranges from 0 to 1. In addition, the pressures measured with protection in front of the caisson (T11, T12, or T13) were normalized by the corresponding values with the same condition but without any protection of the caisson (T01). Then, all the data from the models C12 to C14 were plotted in a single figure.

Figure 14a shows such a representation of the data from T11 and T01 that are marked as blue dots, where p_{T11}/p_{T01} denotes the horizontal wave pressures from T11 normalized by the corresponding pressures from T01. It is very clear that most values of p_{T11}/p_{T01} are less than unity, which implies a reduction of horizontal wave pressure by the protection with armor blocks on the rubble-mounted core. Another noteworthy feature of the data is that data scattering becomes less for relatively smaller values of h_p/h_c . In Figure 14, the black line shows the profile of mean value (μ) plus half of the standard deviation (σ) of the data. Statistically, this curve means the upper 33% value of the data, which gives a more conservative evaluation of the wave pressure, compared to the average of the data.

Figure 14b shows a similar figure drawn by using the data from T12 and T01. Unlike the previous figure, the values of p_{T12}/p_{T01} are greater than unity over the upper part of the caisson, reaching up to approximately 2 at the top of the caisson. This demonstrates that the partially covered caisson receives significantly higher pressures on the unprotected part of the front face than the simple solid caisson, which is probably due to impulsive wave loading on the structure. Meanwhile, the wave pressure ratios over the lower part of the caisson, protected by the armor blocks, are less than unity, as in the previous figure.

Figure 15 represents another similar result for the data from T13 and T01. In this case, the extent of greater value of p_{T13}/p_{T01} than unity is further larger than Figure 14b. In addition, the peak value of p_{T13}/p_{T01} occurs at a slightly lower elevation from the top of the caisson. This is because impulsive wave loading tends to act at a comparatively lower location than T12 as a result of the lower crest level of armor blocks in this case. It is noteworthy that the wave pressures at close to the caisson bottom is almost the same as those in the previous figure.

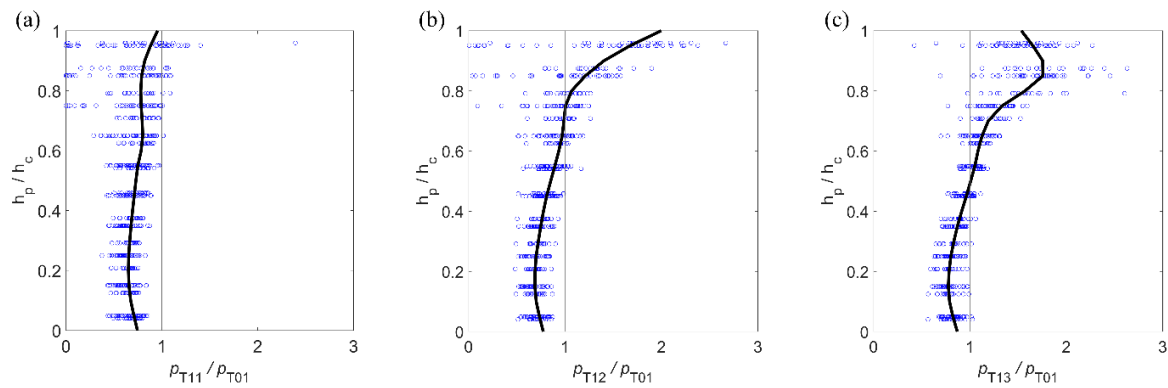


Figure 14. Non-dimensionalized values of the horizontal wave pressures of (a) T11, (b) T12, and (c) T13 with the vertical profile corresponding to $\mu + 0.5\sigma$ of the data.

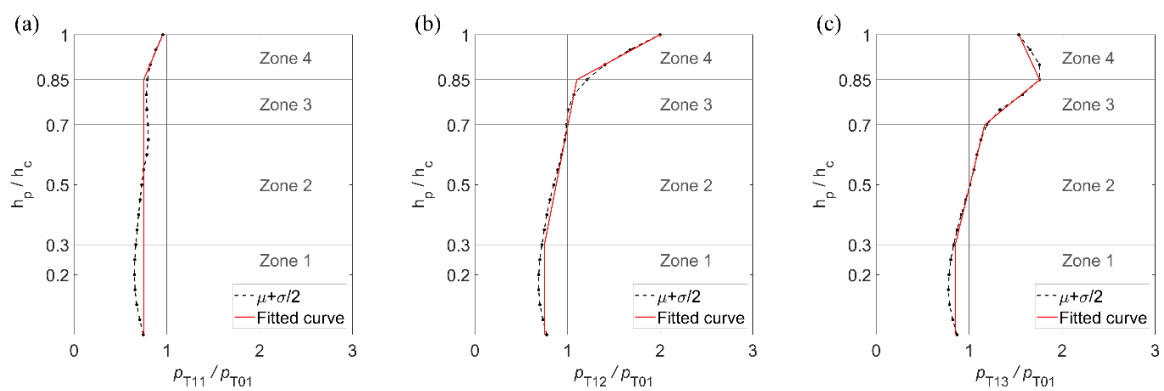


Figure 15. Parameterization of vertical profiles of the normalized wave pressures of (a) T11, (b) T12, and (c) T13.

In Figure 15, the black line shown in Figure 14a–c is presented as a black dotted line in each of the images in Figure 15a–c. Meanwhile, the red line in each of the figures shows a fitted curve that gives a parameterization of the dotted line in Figure 15a–c, which is expressed as an empirical formula in Equations (7)–(9). Hence, values of p_{T11} , p_{T12} , or p_{T13} can be obtained by applying Equations (7)–(9) to p_{T01} , which is readily obtained from Goda’s formula. That is, it is possible to estimate the distribution of horizontal pressure on the caisson covered with armor blocks on the rubble-mounted core, depending on the coverage rates from 70% to 100%.

$$\frac{p_{T11}}{p_{T01}} = \begin{cases} 0.75 & 0 < \frac{h_p}{h_c} \leq 0.85 \\ 0.96 - 1.37\left(1 - \frac{h_p}{h_c}\right) & 0.85 < \frac{h_p}{h_c} \leq 1.0 \end{cases} \quad (7)$$

$$\frac{p_{T12}}{p_{T01}} = \begin{cases} 0.75 & 0 < \frac{h_p}{h_c} \leq 0.3 \\ 1.2 - 0.64\left(1 - \frac{h_p}{h_c}\right) & 0.3 < \frac{h_p}{h_c} \leq 0.85 \\ 2.0 - 6.0\left(1 - \frac{h_p}{h_c}\right) & 0.85 < \frac{h_p}{h_c} \leq 1.0 \end{cases} \quad (8)$$

$$\frac{p_{T13}}{p_{T01}} = \begin{cases} 0.85 & 0 < \frac{h_p}{h_c} \leq 0.3 \\ 1.4 - 0.79\left(1 - \frac{h_p}{h_c}\right) & 0.3 < \frac{h_p}{h_c} \leq 0.7 \\ 2.35 - 3.94\left(1 - \frac{h_p}{h_c}\right) & 0.7 < \frac{h_p}{h_c} \leq 0.85 \\ 1.53 + 1.49\left(1 - \frac{h_p}{h_c}\right) & 0.85 < \frac{h_p}{h_c} \leq 1.0 \end{cases} \quad (9)$$

As illustrated in Figure 15, each of the normalized profiles of wave pressure is discriminated according to the four zones, which are classified as the range of $0 < h_p/h_c \leq 0.3$, $0.3 < h_p/h_c \leq 0.7$, $0.7 < h_p/h_c \leq 0.85$, and $0.85 < h_p/h_c \leq 1.0$, respectively. Note that the value of p_{T11}/p_{T01} is the same as a constant over Zone 1 to 3, but it is expressed as a function of h_p/h_c for Zone 4. Meanwhile, p_{T12}/p_{T01} is a constant only for Zone 1, and it is expressed as a different function of h_p/h_c either for Zones 2 and 3 or Zone 4. Finally, the profile of p_{T13}/p_{T01} is completely different for each of the four zones.

Table 3 shows the mean values of the normalized wave pressures of p_{T11}/p_{T01} , p_{T12}/p_{T01} , and p_{T13}/p_{T01} for the four zones. It is noteworthy that the values in the table are augmented with an increase of h_p/h_c but with a decrease of C_R . Such a trend is very clear in Figure 16, where the abscissa is the coverage rate (C_R) and the ordinate is the adjustment factor (λ_C) that explains the change of horizontal wave pressure due to a different coverage rate. λ_C is basically equivalent to the values of p_{T1x}/p_{T01} with $x = 1, 2, \text{ or } 3$, depending on the coverage rate. Then, it is possible to draw fitted lines for each of the four zones that follow the data, as shown in Figure 16, and to obtain simplified relationships between λ_C and C_R based on the fitted lines, as suggested in Equation (10).

$$\lambda_C = \begin{cases} \max\{0.75, 1.55 - C_R\} & 0 < h_p/h_c \leq 0.3 \\ 1.58 - 0.83C_R & 0.3 < h_p/h_c \leq 0.7 \\ 3.05 - 2.3C_R & 0.7 < h_p/h_c \leq 0.85 \\ \min\{1.6, 5.82 - 4.97C_R\} & 0.85 < h_p/h_c \leq 1.0 \end{cases} \quad \text{for } 0.7 \leq C_R \leq 1.0 \quad (10)$$

Table 3. Mean values of the normalized horizontal wave pressures from Zone 1 to 4.

	Zone 1	Zone 2	Zone 3	Zone 4
p_{T11}/p_{T01} ($C_R = 1.0$)	0.75	0.75	0.75	0.86
p_{T12}/p_{T01} ($C_R = 0.85$)	0.75	0.87	1.05	1.55
p_{T13}/p_{T01} ($C_R = 0.7$)	0.85	1.00	1.46	1.65

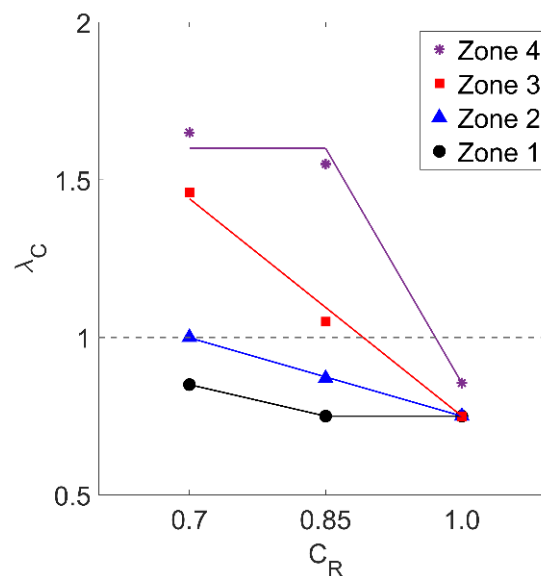


Figure 16. The adjustment factor of horizontal pressure depending on different coverage rates.

Figure 17 shows a comparison of the horizontal wave forces calculated by using Equation (10) with the measurement, which gives good agreement between the calculation and the measurement. In particular, compared to the prediction by Takahashi’s formula presented in Figure 13, the suggested equation provides apparently better performance in predicting the measured forces.

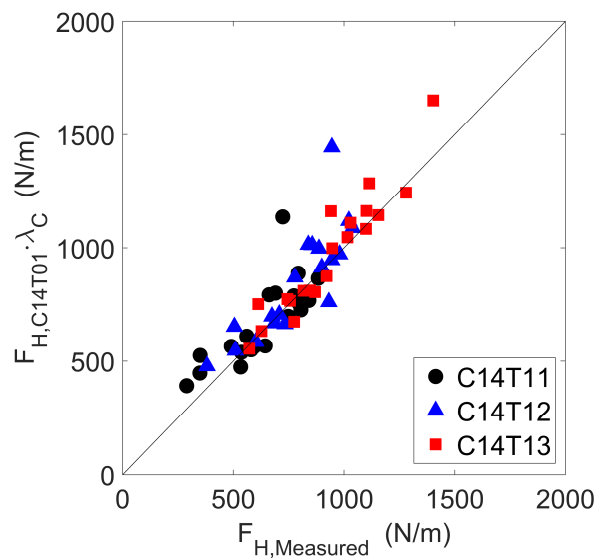


Figure 17. Comparison of horizontal wave forces from the experiment with Equation (10).

4. Influence of Shoulder Width of the Armor Layer

4.1. Experimental Conditions with Different Shoulder Widths of the Armor Layer

The three models investigated in the previous chapter have the same shoulder width of $G_c = 0.15$ m, which corresponds to two times of the nominal diameter of the tetrapod that is used in the experiment. However, in some cases, more than two armor units are placed on the shoulder to further reduce the wave loading on the caisson. In order to examine such an influence, additional experiments were carried out with a wider shoulder width than C14. Figure 18 is a schematic diagram illustrating the difference of the two additional models, termed C17 and C18, from C14. The shoulder width of the C17 and C18 models are $G_c = 0.225$ m and 0.30 m, which correspond to three and four times the nominal diameter of the tetrapod, respectively. Except for the shoulder width, all the other geometrical parameters of the two models were the same as those in C14. Table 4 summarizes the parameters of the two additional models. For the C17 and C18 models, only the case with full protection in front of the caisson (T11) was subject to the experiment. This is because partial protection (T12 or T13) would not be a recommended design concept, which results in a significant increase of the horizontal wave loading on the top disclosed section of the caisson, as elucidated in the previous chapter.

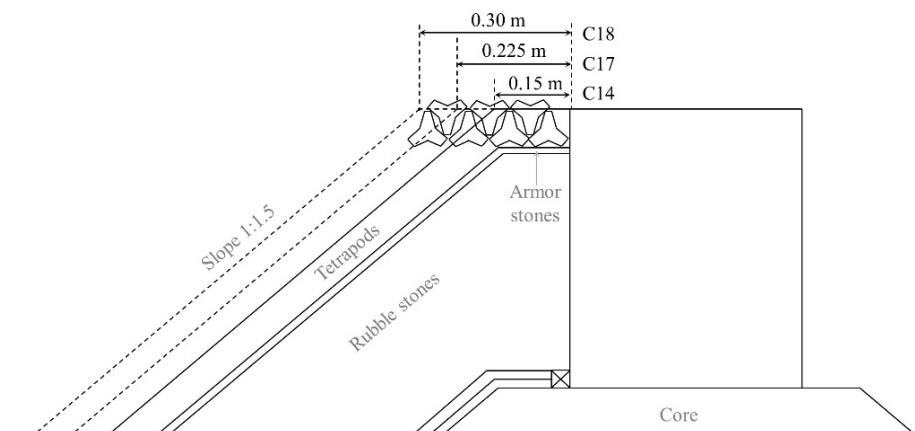


Figure 18. Illustration of three models with different shoulder widths (G_c) of the armor layer.

Table 4. Values of the geometrical parameters of the two models of wider shoulder width.

Model ID	h (m)	h_M (m)	h_c (m)	G_c (m)	R_c (m)
C17	0.50	0.10	0.60	0.225	0.20
C18	0.50	0.10	0.60	0.300	0.20

4.2. The Effect of Shoulder Widths on the Measured Forces and Pressures

First, the effect of shoulder width was investigated for the wave forces obtained by integration of the horizontal pressures over the front face of the caisson. Figure 19 shows the horizontal wave forces on the caisson of C17 or C18 models ($F_{H,C17}$ or $F_{H,C18}$) that are compared with the corresponding forces on C14 model ($F_{H,C14}$). In general, the wave forces likely decrease as the shoulder width increases, especially when the forces are comparatively small. As the magnitude of measured forces increases, the effect of the shoulder width becomes less significant.

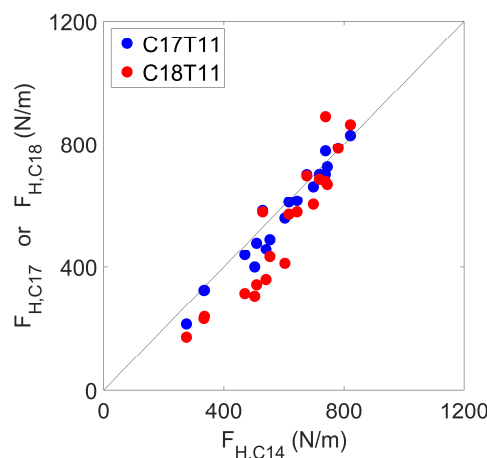


Figure 19. Comparison of the integrated wave forces on the C17 and C18 models with the C14 model.

Then, pressure distributions under different shoulder widths were compared as shown in Figure 20, which shows the measured pressures of either the C17 or C18 model that are normalized by the corresponding values of the C14 model. Although data scattering is comparatively larger for higher values of h_p/h_c , the mean profile of the normalized data, presented as a black line in the figure, apparently illustrates a decrease of the wave pressures with an increase of the shoulder width, especially over the upper part of the caisson.

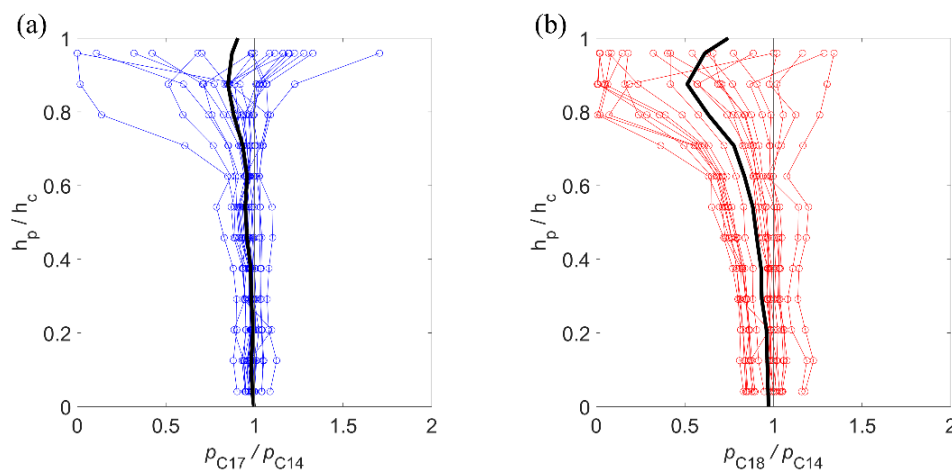


Figure 20. Normalized values of the horizontal wave pressures of the (a) C17 and (b) C18 models with the vertical profile corresponding to the mean value (μ) of the data that are illustrated as a black line.

The two normalized pressure profiles in Figure 20 are shown together in Figure 21, where λ_W is the adjustment factor for horizontal wave pressure considering the effect of shoulder width. λ_W is basically equivalent to the values of p_{C17}/p_{C14} or p_{C18}/p_{C14} . As illustrated in Figure 21, the normalized pressure profiles can be simplified as fitted lines that vary according to the three zones of $0 < h_p/h_c \leq 0.7$, $0.7 < h_p/h_c \leq 0.85$, and $0.85 < h_p/h_c \leq 1.0$, respectively. These three zones are correspondent to Zone 1 plus Zone 2, Zone 3, and Zone 4 described in Section 3.4, respectively.

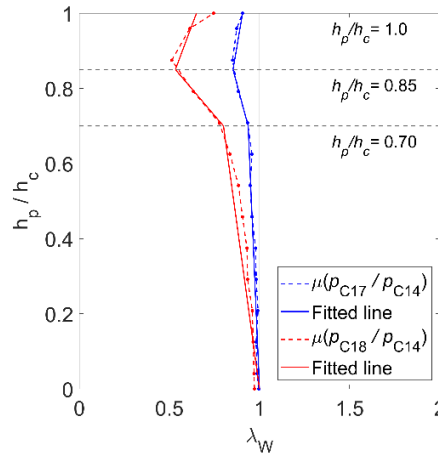


Figure 21. Vertical profiles of the wave pressure of C17 and C18 normalized by the case of C14.

4.3. Parameterization of the Effect of Shoulder Width

Although we obtained fitted lines that explain the adjustment factor for the effect of shoulder width, it is only usable for the specific shoulder width corresponding to C17 or C18 models. Hence, it is required to develop a methodology that can be applicable for an arbitrary shoulder width. In this respect, there have been efforts to find a parameter that shows a recognizable relationship between the modification factor λ_W and the shoulder width. Then, it was disclosed that λ_W shows a decreasing trend when it is represented as a function of a dimensionless parameter, $G_c/L \cdot \xi$, as illustrated in Figure 22. The figure contains three panels that show the data points corresponding to $h_p/h_c = 0.7, 0.85$, and 1.0 , respectively. Those data points at each of the three values of h_p/h_c come from interpolation/extrapolation of all the individual profiles of p_{C17}/p_{C14} and p_{C18}/p_{C14} , which are already shown in Figure 20. The black solid lines in each panel of Figure 22 denote suggested simplification of the data, the formulations of which are given in Equations (11)–(13). It is noteworthy that the simplification of λ_W is given as a constant for $G_c/L \cdot \xi > 0.28$ for all the three values of h_p/h_c . Although there exists no available data in the present experiment over this range, we may conjecture that values of λ_W are likely to further decrease down to zero with any increase of $G_c/L \cdot \xi$. However, λ_W is assumed to be constant when $G_c/L \cdot \xi > 0.28$ in view of the conservative consideration regarding the effect of shoulder width on wave force reduction.

$$\lambda_W = \begin{cases} 1.0 & 0 < G_c/L \cdot \xi \leq 0.15 \\ -4.62G_c/L \cdot \xi + 1.69 & 0.15 < G_c/L \cdot \xi \leq 0.28 \\ 0.4 & 0.28 < G_c/L \cdot \xi \end{cases} \quad \text{when } h_p/h_c = 0.7 \quad (11)$$

$$\lambda_W = \begin{cases} 1.0 & 0 < G_c/L \cdot \xi \leq 0.15 \\ -7.46G_c/L \cdot \xi + 2.12 & 0.15 < G_c/L \cdot \xi \leq 0.28 \\ 0.03 & 0.28 < G_c/L \cdot \xi \end{cases} \quad \text{when } h_p/h_c = 0.85 \quad (12)$$

$$\lambda_W = \begin{cases} 1.0 & 0 < G_c/L \cdot \xi \leq 0.15 \\ -6.85G_c/L \cdot \xi + 2.03 & 0.15 < G_c/L \cdot \xi \leq 0.28 \\ 0.11 & 0.28 < G_c/L \cdot \xi \end{cases} \quad \text{when } h_p/h_c = 1.0 \quad (13)$$

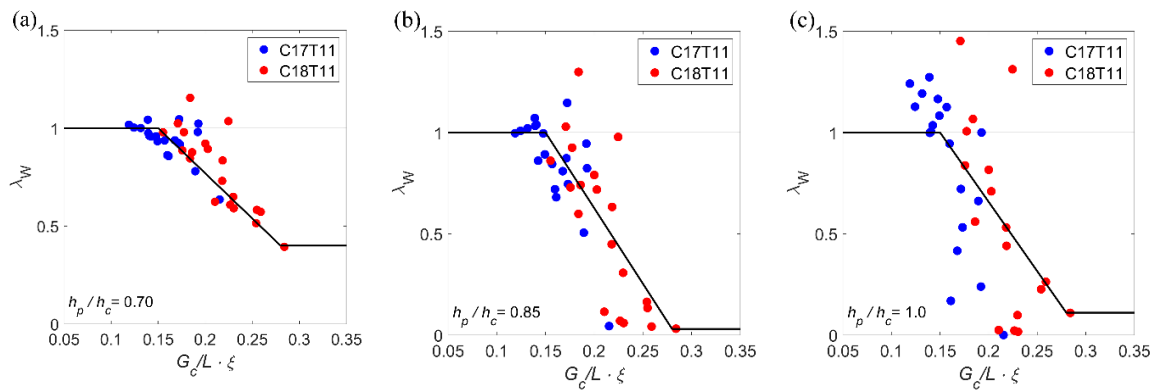


Figure 22. Values of λ_W as a function of $G_c/L * \xi$ at (a) $h_p/h_c = 0.7$, (b) $h_p/h_c = 0.85$, and (c) $h_p/h_c = 1.0$.

Based on the three equations above, formulations of the modification factor (λ_W) can be obtained for the entire range of h_p/h_c from zero to unity, as tabulated in Table 5. The value of λ_W is unity regardless of h_p/h_c when $G_c/L \cdot \xi$ is less than or equal to 0.15. In the range of $0.15 < G_c/L \cdot \xi \leq 0.28$, λ_W is represented as a function of both $G_c/L \cdot \xi$ and h_p/h_c with different coefficient values depending on the ranges of h_p/h_c . Finally, when $G_c/L \cdot \xi$ is greater than 0.28, λ_W is expressed as a sole function of h_p/h_c .

Table 5. The reduction factors due to the shoulder width (λ_W) of the armor layer.

	$G_c/L \cdot \xi \leq 0.15$	$0.15 < G_c/L \cdot \xi \leq 0.28$	$0.28 < G_c/L \cdot \xi$
$0.85 < h_p/h_c \leq 1.0$	1.0	$-10.6(G_c/L \cdot \xi - 0.24) + 4.11(G_c/L \cdot \xi - 0.15) \frac{h_p}{h_c}$	$-0.42 + 0.53 \frac{h_p}{h_c}$
$0.7 < h_p/h_c \leq 0.85$	1.0	$8.62(G_c/L \cdot \xi - 0.035) - 18.9(G_c/L \cdot \xi - 0.15) \frac{h_p}{h_c}$	$2.13 - 2.47 \frac{h_p}{h_c}$
$h_p/h_c \leq 0.7$	1.0	$1.0 - 6.58(G_c/L \cdot \xi - 0.15) \frac{h_p}{h_c}$	$1.0 - 0.85 \frac{h_p}{h_c}$

Figure 23 presents two examples showing a comparison of the measured pressure profiles from either the C17T11 or C18T11 model with the calculation by multiplying λ_W to the pressure profiles of C14T11. As shown in Figure 23, the calculated profiles generally agree well with the measured profiles, indicating that the effects of the shoulder width are properly taken into account with the modification factor λ_W .

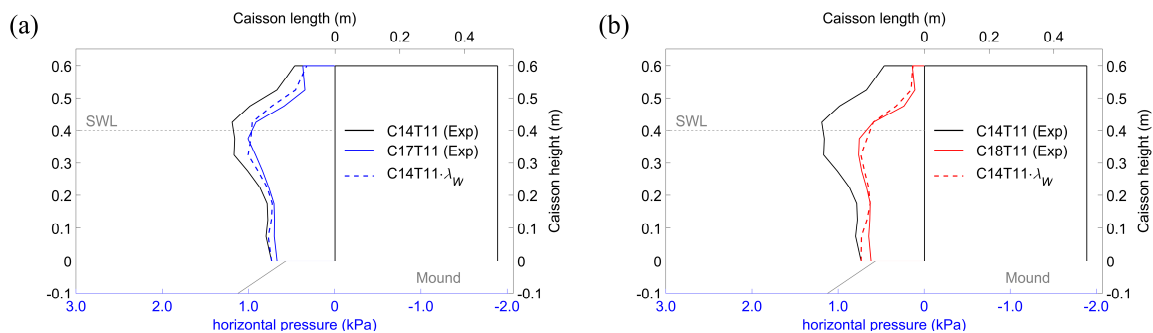


Figure 23. Comparison of vertical profiles of horizontal wave pressure from the measurement of (a) C17T11 and (b) C18T11 with the calculated results obtained by applying λ_W to C14T11.

4.4. Verification of Applying the Two Modification Factors Together

For the entire 20 wave conditions of the C17T11 and C18T11 models, the measured wave forces are compared with the forces of C14T01 that are multiplied by λ_C and λ_W . Figure 24 shows such a comparison of the horizontal wave forces acquired by integration of the pressures along the caisson height between the measurement and estimation. The agreement between the measured and calculated wave forces is fairly good, and the correlation coefficient (R) is 0.93. This implies that the two modification factors provide a reasonable estimation of the wave forces on a caisson that is partially covered with armor blocks of arbitrary shoulder width on the rubble-mounted core caisson.

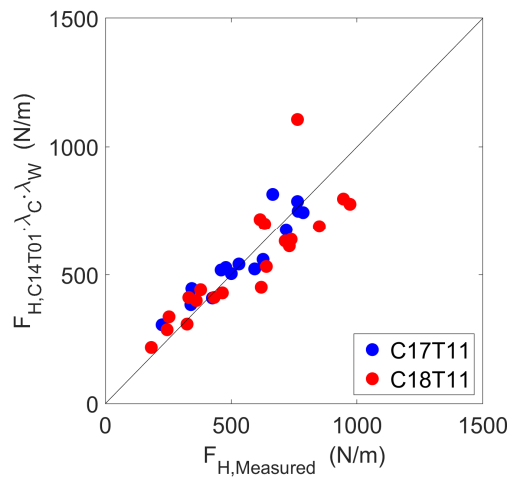


Figure 24. Comparison of measured horizontal wave forces with the calculation by using λ_C and λ_W .

5. Conclusions

This paper experimentally investigated characteristics of the wave loading on the front wall of the caisson covered with armor blocks on the rubble-mounted core. Analysis of the experimental data showed that horizontal wave pressure on the caisson apparently increases when the caisson was not fully covered. This is because impulsive loading, incurred by wave breaking over the fore slope of the caisson, is likely to act on the unprotected section of the caisson. This demonstrates the importance and necessity of full protection of the caisson up to the crest level, as imperfect protection may result in even greater wave loading than a simple solid caisson without any protection.

For seeking a quantification of the measured pressure under different coverage rates, the measured wave pressure was first compared with a formula suggested by Takahashi et al. [11], although it has been suggested for a caisson that is entirely protected by armor blocks without rubble-mounted core. In general, the formula tends to overestimate the measured pressure on the lower part of the caisson that is well protected, whereas it underestimates the upper part of the caisson that is unprotected by the armor blocks. Then, we suggest a new formula based on the parameterization of vertical profiles of the measured horizontal pressure. The main idea of the parameterization is to find a representative profile of the normalized pressure as a function of relative vertical position along the front wall of the caisson (h_p/h_c), from which an adjustment factor (λ_C) was introduced considering the effects of the coverage rate (C_R). The influence of the shoulder width of the armor layer was also examined, which showed a decrease of the wave pressures on the caisson with the increase of the shoulder width, especially over the upper part of the caisson. In order to quantify such an influence due to the shoulder width, another adjustment factor (λ_W) has been proposed, which is presented as the functions of two parameters $G_c/L * \xi$ and h_p/h_c .

The adequacy of the two suggested that the adjustment factors were verified by using the experimental data, indicating that the factors can be used to estimate horizontal wave pressures on a

caisson that is protected by armor blocks on the rubble-mounted core within the ranges of physical parameters investigated in this study.

Author Contributions: Conceptualization, S.-H.O.; methodology, S.-H.O. and J.-S.L.; software, S.-H.O. and J.-S.L.; validation, S.-H.O.; formal analysis, J.-S.L.; investigation, S.-H.O. and J.-S.L.; data curation, J.-S.L.; writing—original draft preparation, review and editing, S.-H.O. and J.-S.L.; funding acquisition, S.-H.O. All authors have read and agreed to the published version of the manuscript.

Funding: This study is part of a research project titled “Development of Design Technology for Safe Harbor from Disasters”, which is funded by Ministry of Oceans and Fisheries of Korea (Project No. 20180323/PM61720). The APC was supported by the research project (PG51880) of Korea institute of Ocean Science and Technology.

Conflicts of Interest: The authors declare no conflict of interest.

References

1. Goda, Y. New Wave Pressure Formulae for Composite Breakwaters. In Proceedings of the 14th International Conference on Coastal Engineering, Copenhagen, Denmark, 24–28 June 1974; pp. 1702–1720. [[CrossRef](#)]
2. Goda, Y. *Random Seas and Design of Maritime Structures*, 3rd ed.; World Scientific: Singapore, 2010; ISBN 978-981-4282-39-0. [[CrossRef](#)]
3. Takahashi, S. Design of vertical breakwaters. In *Random Seas and Design of Maritime Structures; PHRI Ref. Doc. Nr 34*; World Scientific Publishing: Singapore, 2002. [[CrossRef](#)]
4. Takahashi, S.; Tanimoto, K.; Shimosako, K. Wave and block forces on a caisson covered with wave dissipating blocks. *Rep. Port Harb. Res. Inst. Yokosuka Jpn.* **1990**, *30*, 3–34.
5. Takahashi, S.; Shimosako, K.; Kimura, K.; Suzuki, K. Typical Failures of Composite Breakwaters in Japan. In Proceedings of the 27th International Conference on Coastal Engineering, Sydney, Australia, 16–21 July 2000; pp. 1899–1910. [[CrossRef](#)]
6. Oh, S.-H.; Lee, J.; Lee, J.-S. Experimental Investigation of the Wave Force on the Caisson According to Different Coverage of Armor Units. In *Proceedings of the International Conference on Asian and Pacific Coasts*; Springer: Singapore, 2019; pp. 987–993. [[CrossRef](#)]
7. Hitachi, S. Case study of breakwater damages Mutsu-Ogawara Port. In *Proceedings of the Workshop on Wave Barriers in Deepwaters*; Port and Harbor Research Institute: Yokosuka, Japan, 1994; pp. 308–331.
8. Allsop, N.W.H.; McKenna, J.E.; Vicinanza, D.; Whittaker, T.T.J. New design methods for wave impact loadings on vertical breakwaters and seawalls. In Proceedings of the 25th International Conference on Coastal Engineering, Orlando, FL, USA, 2–6 September 1996; pp. 2508–2521. [[CrossRef](#)]
9. Takayama, T.; Tsujio, D.; Yasuda, T. Estimation of Expected Sliding Distance of a Caisson Affected by Damage of Armor Concrete Blocks. In Proceedings of the 31st International Conference, Hamburg, Germany, 31 August–5 September 2008; pp. 3645–3654. [[CrossRef](#)]
10. Mase, H.; Tsujio, D.; Yasuda, T.; Mori, N. Stability analysis of composite breakwater with wave-dissipating blocks considering increase in sea levels, surges and waves due to climate change. *Ocean Eng.* **2013**, *71*, 58–65. [[CrossRef](#)]
11. Takahashi, S.; Ohki, Y.; Shimosako, K.; Isayama, S.; Ishinuki, K. *Seawall Failures by Typhoon 9918 and Their Reproduction in Wave Flume Experiments*; Technical Note; The Port and Harbour Research Institute, Ministry of Transport, Japan: Yokosuka, Japan, 2000; Volume 973, pp. 3–50.
12. Oh, S.-H. Two-dimensional wave flume with water circulating system for controlling water level. *J. Korean Soc. Coast. Ocean Eng.* **2018**, *30*, 337–342. [[CrossRef](#)]
13. Oh, S.-H.; Lee, J.-S.; Lee, J. Introduction to Physical Experiment Building of Kiost in Busan. In *Proceedings of the International Conference on Asian and Pacific Coasts*; Springer Nature: Singapore, 2019; pp. 221–226. [[CrossRef](#)]
14. Oh, S.-H.; Ji, C.-H. Simultaneous measurement of wave forces and pressures on a double-chamber perforated caisson. *Meas. Sci. Technol.* **2019**, *30*, 105801. [[CrossRef](#)]

